Phase transition and abnormal compressibility of lanthanide silicate with the apatite structure

F. X. Zhang, M. Lang, J. M. Zhang, Z. Q. Cheng, Z. X. Liu, J. Lian, and R. C. Ewing

Phys. Rev. B **85**, 214116 — Published 18 June 2012

DOI: 10.1103/PhysRevB.85.214116

Phase Transition and Abnormal Compressibility of Lanthanide Silicate with the Apatite Structure

F.X. Zhang[1], M. Lang[1], J.M. Zhang[1], Z.Q. Cheng[2], Z.X. Liu[3], J. Lian[4], and R.C. Ewing[1*]

[1]*Department of Earth and Environmental Sciences, University of Michigan, Ann Arbor, MI 48109*

[2]*Department of Geosciences, SUNY Stony Brook, NY 11794*

[3]*Geophysical Laboratory, Carnegie Institution of Washington, Washington, D.C. 20015*

[4]*Department of Mechanical, Aerospace & Nuclear Engineering, Rensselaer Polytechnic Institute, Troy, NY 12180*

The lanthanide silicate, $La_{9.33}Si_6O_{26}$, which has the hexagonal apatite structure ($P6_3/m$), was investigated at high pressure. A subtle phase transition was observed at ~13.3 GPa by *in situ* synchrotron x-ray diffraction (XRD) and confirmed by infrared absorption (IR) and Raman scattering measurements. The high-pressure phase has a structure similar to that of the initial hexagonal apatite structure, but the symmetry is reduced to $P6_3$ through the displacement of one oxygen site and tilting of the SiO_4 tetrahedra. Interestingly, the high-pressure phase has an abnormally lower compressibility, which is caused by the change in symmetry that allows the tilting of the SiO_4 tetrahedra, and the bulk modulus of the high-pressure phase is only half that of the apatite structure.

Introduction

Natural calcium phosphate apatite, $Ca_{10}(PO_4)_6(F,Cl,OH)_2$, is an important mineral in geochemistry[1], biology[2] and the materials science of actinides[3,4]. Recently, lanthanide silicates with the apatite structure have been widely investigated due to their potential use as catalysts[5], fast oxygen ion conductors, luminescent materials[6,7] and as actinide waste forms[4] As a new class of oxygen ion conductors, lanthanide silicate apatite has a "super" oxygen conductivity (2.42×10^{-4} $S\ cm^{-1}$ at 300 °C) at moderate temperatures, which is even higher than that of stabilized zirconia[8] (3.75×10^{-6} $S\ cm^{-1}$ at 300 °C). Most of the lanthanide silicate apatites are isostructural with calcium phosphate ($P6_3/m$). The structure is relatively open, and the SiO_4 tetrahedra are not connected to one another, but form a circular array with translations along the *c*-axis. There are four oxygen sites in the apatite structure, of which three surround Si, forming SiO_4 tetrahedra, and the forth oxygen site lies in channels, which parallel the c-axis. When the large cation sites are occupied with trivalent cations only, such as lanthanides, one site (*4f*) will be not fully occupied in order to maintain charge balance, and a non-stoichiometric chemical composition results. In addition, previous investigations have shown that the anions in the channels of non-stoichiometric systems are significantly disordered as interstitial sites, and the interstitial oxygen ions in these channels are responsible for the high oxygen ion conductivity in apatite-type silicates[9-11]. However, details of the high oxygen ion conduction mechanism, and the influence of cation vacancies on this process, are not yet fully understood[12].

Due to the wide variety of applications and unique oxygen ion conduction mechanism, the structure of lanthanide silicate apatite has been extensively studied by various experimental methods, such as single crystal and powder x-ray diffraction (XRD)[13, 14], neutron diffraction[12, 15], nuclear magnetic resonance (NMR)[9], and optical spectroscopy[16-18], as well as theoretical

modeling[19]. There are, however, still unresolved issues related to the lattice symmetry, the accuracy of parameter values and their influence on critical properties[13, 15, 17, 19]. The structure of apatite is relatively open, and the structural response to external pressure is of particular interest. Up to now, there are only a limited number of data available, which focus on the response of the phosphate apatite structure, and all are at relatively low pressures[21, 22]. In this paper, the structural response of $La_{9.33}Si_6O_{26}$ with the apatite structure has been studied at pressures up to 38 GPa. A structural transformation was independently observed by *in situ* XRD, Raman scattering and IR absorption measurements. The phase transformation is characterized by a reduction in symmetry that leads to an unexpected softness of the high-pressure phase. High-pressure phases are normally denser than the corresponding state at ambient conditions because of the shortening of distance among atoms. High-pressure phases are thus expected to be "stiffer" than the ambient forms, though some solids may show anisotropic compressibility. As far as we know, materials with softer high-pressure phase have not been previously described.

Experimental Section

The silicate apatite was prepared by a high-temperature, solid-state reaction method. Pure La_2O_3 (Alfa Asear, >99.9%) and SiO_2 (Alfa Asear, 99.8%) powders were thoroughly mixed in the composition of $La_{9.33}Si_6O_{26}$ and pressed into a pellet, and then calcined at temperature of 1300-1600°C for several days with intermediate regrinding and shaping. A single phase of the apatite structure was confirmed by XRD measurements. High-pressure experiments were performed with symmetric-type diamond anvil cells (DAC) at room temperature with hardened stainless steel gaskets. For the XRD and Raman measurements, a methanol/ethanol mixture (4/1 in volume) was used as a pressure medium. The *in situ* XRD patterns and infrared spectra were collected at the X17C and U2A stations of National Synchrotron Light Source, Brookhaven

National Laboratory, respectively. A monochromatic x-ray beam with an energy of 30.5 keV was used for XRD measurements. The diffraction pattern intensities were integrated from the CCD detector images using the program FIT2D[23]. The facility parameters are calibrated with CeO_2 powder as an external standard. The unit cell parameters were derived from the patterns by Rietveld refinement method using the program FullProf[24]. The pressure in all of the experiments was measured by the ruby fluorescence method [25]. Raman scattering measurements were conducted with a modified Spex1250 spectrometer attached to a liquid nitrogen cooled CCD detector. Green light (532.1 nm) from a Verdi solid-state laser was used as the activation source. The IR data were collected in the far-IR (FIR) region (<700 cm^{-1}) with a helium-cooled Ge detector and in the middle-IR (MIR) (>700cm^{-1}) with a Bruker IRscope II system. The pressure medium for MIR and FIR measurements are KBr crystal and vaseline, respectively.

Results and Discussion

Powder XRD measurement at ambient conditions was done in synchrotron beam without diamond anvil cell, confirming that the synthetic sample was a well crystallized and a single phase of apatite (*P6₃/m*). However, a non-stoichiometric composition of $La_{9.0}Si_6O_{26}$ was derived from Rietveld analysis, and the cation vacancy is mainly on the *4f* site. With an increase of pressure, the x-ray diffraction patterns suggest that the apatite sample retains its crystalline structure up to the maximum pressure of 38 GPa (Fig. 1), but all the diffraction peaks have significantly reduced intensities at 38 GPa with an obvious broadening of the peaks. In addition, we observed two different types of change in the XRD patterns at high pressures. First, starting at 13.3 GPa, there is an clear increase in the intensity for the first diffraction maximum (010) at low 2 □ angle. Second, two diffraction peaks, at a 2 □ of 6.5-7.5° with moderate intensity in the XRD pattern at 13.3 GPa, split into two peaks, and the two original peaks are replaced with two

new ones in the XRD patterns above 13.3 GPa (Fig. 1). These changes are, in fact, caused by a subtle phase transition of the apatite structure at high pressure. The similar character of the diffraction profiles at low and high pressures suggests that the structural modification of the apatite structure at high pressures is, in fact, very limited. The measured XRD patterns at 13-15 GPa also indicated that the pressure-induced structural change of apatite is rapid, and we only able to capture the coexistence of the low- and high-pressure structures of the silicate apatite in a single XRD pattern at 13.3 GPa. The intensity of the two diffraction maxima (002) and (012) is reduced with increasing pressure, and both peaks are finally replaced by two new diffraction maxima with slightly lower d-spacings. There might be also a change in other diffraction maxima at higher 2 □ range, but this is difficult to observe because of peak overlap and/or weak peak intensities. The structural transition was complete at 15.2 GPa. Despite the changes in the patterns at pressure above 13.3 GPa, all of the diffraction maxima observed above 13.3 GPa can also be well indexed with a hexagonal unit cell. The *a/b*-lattice parameters of the high-pressure phase change continuously from the low-pressure phase, but the *c*-parameter shows an obvious discontinuity from the low-pressure phase with increasing pressure. The sudden decrease in the *c*-lattice parameter is probably the cause of the splitting of the (002) and (012) diffraction maxima in the XRD pattern at 13.3 GPa. Through Rietveld-like refinement, we found that the XRD patterns of the high-pressure phase do not give a good refinement in the original $P6_3/m$ space group, especially for the relatively high intensity of the first diffraction maximum. A detailed analysis of the indexing and refinement-like fitting of the XRD patterns and subsequent spectroscopic studies confirmed that the high-pressure phase must have a lower symmetry as compared with the low-pressure phase. In fact, several low-symmetry structure models have been proposed for some complex apatite compounds with mixed occupancy in cation and/or

anion sites[14]. In addition to $P6_3/m$, other possible lower symmetry space groups for apatite structures include: hexagonal $P6_3$, $P\text{-}6$, trigonal $P\text{-}3$, and monoclinic $P2_1/m$, $P2_1/b$ and $P2_1$. The structural details of various apatite compounds have been recently summarized by White et al.[14]. Since XRD results of this study indicate that the high-pressure phase of $La_{9.33}Si_6O_{26}$ has the same extinction rules as those of the low-pressure phase, $P6_3/m$, the most probably structure for the high-pressure phase is $P6_3$. The refinement of the high-pressure phase with structural model[26] in space group of $P6_3$ yields a much better fit to the diffraction data. The XRD patterns of $La_{9.33}Si_6O_{26}$ at 1 bar and 15.2 GPa refined with space group of $P6_3/m$ and $P6_3$, respectively, are shown in Fig. 2a and the detailed structural data are listed in Table I. The refined unit cell parameters and volume at various pressures are plotted in Figs. 2b-e. The phase transition at 13.3 GPa is accompanied by a volume decrease (~3%). The volume collapse at the critical pressure is mainly caused by the sudden decrease of the *c*-parameter (~2.3%). The pressure dependence of *c*/*a* value is shown in Fig. 2e. In the same polymorph, *c/a* increases nearly linearly with pressure, which demonstrates that the apatite structure is more easily compressed in the *a*-*b* plane. In other words, the channels created by the oxygen atoms shrink more easily than along the *c*-axis. The *c*/*a* ratio as function of pressure has an obvious discontinuity during the phase transition with a higher slope for the high-pressure phase indicating that the compression along the *c*-axis is more restricted than for the low-pressure phase. A quantitative analysis of the compressibility was obtained by fitting the P-V curves with Birch-Murnaghan equation of state (Fig. 2b). In order to make the fitting simple and obtain a comparable bulk modulus for the two phases, the pressure derivative at zero pressure B_0' is fixed at 4. Because of the poor data quality of the XRD profile at 38 GPa, the unit cell volume at this pressure deviates too much from the predicted P-V curve and is thus excluded from the fitting of equation of state. The bulk modulus, B_0, from the fit is

145.8 GPa for the low-pressure phase and 72.5 GPa for the high-pressure phase. The bulk modulus of the high-pressure phase is only half that of the low-pressure phase, and this is very unusual. The high-pressure phase of materials is usually denser than the corresponding low-pressure phase, consistent with an increase of bond stiffness. A high-pressure phase is thus expected to have a larger bulk modulus than the corresponding low-pressure phase. To our knowledge, simple oxides, as well as more complex structures, follow this rule without exception. The bulk moduli of low- and high-pressure polymorphs of some representative simple oxides and silicates are listed in Table II. All the high-pressure structures have a distinctly greater bulk modulus than their low-pressure forms, especially for zirconia[30, 31], the cotunnite-type high-pressure phase being the hardest known oxide.

Abnormal lattice behavior has been reported previously for other materials, such as anisotropic thermal vibration-induced negative expansion in tungsten oxides[36] and water intercalation-induced lattice expansion of $La_2Zr_2O_7$ pyrochlore at high pressures[37]. The abnormal compressibility of the high-pressure phase of lanthanide silicate apatite has a different origin. A detailed analysis of the different structure models of apatite suggests that the softness of the high-pressure phase is due to the special arrangement and tilting of the SiO_4 tetrahedra. In the low-pressure phase, the SiO_4 tetrahedron consists of three independent oxygen atoms (O1-O3), in which the O3 atoms on *12i* has two sites forming one edge of the tetrahedron parallel to the *a-b* plane. During compression, this SiO_4 tetrahedron edge remains constantly parallel to the *a-b* plane (right bottom of Fig. 1). In the low symmetry ($P6_3$) high-pressure phase, there are additional La and O sites, and four independent oxygen atoms (O1-O4) form the SiO_4 tetrahedron. The O3 oxygen in the low-pressure phase ($P6_3/m$) splits into two different *6c* sites, and the edge (O3-O4) of the SiO_4 tetrahedron no longer parallels to the *a-b* plane. The

elimination of the symmetry restriction on the SiO_4 tetrahedron leads to greater degree of freedom and allows tilting of SiO_4 tetrahedra in the high-pressure phase. As a result, the neighboring SiO_4 tetrahedra are closer to one another. The reduction of symmetry results a sudden shrinkage of the unit cell along the *c*-axis at high pressures.

In situ optical spectroscopy measurements confirmed the pressure-induced phase transition for $La_{9.33}Si_6O_{26}$ apatite and the lower symmetry of the high-pressure phase. Fig. 3a shows the Raman spectra at selected pressures. There are obvious changes in the vibrational behavior at pressures between 12.5 and 14.8 GPa. At least three new Raman modes are apparent at a wavenumber of ~540, 580 cm^{-1} and below 100 cm^{-1}, and occur simultaneously with the disappearance of one mode centered at ~160 cm^{-1}. Previous Raman investigations of apatite[17, 18] assigned all the bands below 350 cm^{-1} as external (translational and rotational) modes, whereas, bands between 350 and 600 cm^{-1} were considered to be internal bending modes. The SiO_4 internal stretching modes have the highest frequencies above 800 cm^{-1}. Some of the low frequency external modes are related to La-O bonds, and the appearance of a new mode below 100 cm^{-1} at pressure above 12.5 GPa can be interpreted as being the result of the splitting of one La site in the $P6_3$ unit cell. The new modes with frequencies of ~540 and ~580 cm^{-1} are the result of the asymmetric bending mode of O-Si-O. Since the O3 atom in $P6_3/m$ degenerates into two oxygen sites in the high-pressure phase, the appearance of new asymmetry bending modes is expected. The modes between 800 and 1000 cm^{-1} are the stretching modes of SiO_4 tetrahedron, and the asymmetric stretching modes have higher frequencies. The additional modes above 1000 cm^{-1} in the high-pressure Raman spectra are caused by the methanol/ethanol pressure medium. Though it is difficult to identify the appearance of new symmetric or asymmetric stretching modes due to overlap, the observed intensity increase of the asymmetric stretching modes of SiO_4 at high pressures is also

in agreement with the low symmetry structure model for the high-pressure phase. The frequency *vs*. pressure dependence of all the Raman active modes of apatite is shown in Fig. 3b. Besides the appearance of three new modes previously discussed, some of the modes show an obvious change in slope during the phase transition, which is related to the discontinuous change of the *c* lattice parameter.

The IR spectra of the $La_{9.33}Si_6O_{26}$ apatite structure are shown in Fig.4. Similar to the Raman spectra, the IR active modes below 350 cm^{-1} are external modes due to the rotation and translation of SiO_4 tetrahedra. These bands are relatively broad, and the change caused by the phase transition is not clearly evident. In contrast, the change of bending modes between 350 and 600 cm^{-1} is obvious. At least two of the symmetric bending modes at lower frequencies have decreased intensities at high pressure and are replaced by two or three new weak modes of different frequencies. The latter are probably caused by the asymmetric bending modes in relation to the degradation of symmetry. The MIR spectrum between 800-1200 cm^{-1} contains several symmetric and asymmetric stretching modes. The considerable amount of overlap does not allow for a detailed analysis of individual peaks, but the observed intensity changes with increasing pressure are probably caused by the interplay of disappearing and appearing modes related to the low- and high-pressure phases.

The pressure medium of M/E in XRD and Raman measurements did solidify above 10-12 GPa, but the pressure-induced phase transition in $La_{9.33}Si_6O_{26}$ apatite is not caused by the non-hydrostatic conditions. The good agreement of the transition pressure in these independent experiments with different pressure media confirm that the transition is not related to the type of pressure medium. The pressure-induced changes observed in both the Raman and IR spectra

support the XRD findings of a phase transformation driven by a lower symmetry high-pressure phase.

Although it is widely accepted that the apatite structure at ambient conditions is of high symmetry with space group of $P6_3/m$, there is some controversy over the existence of alternative low-symmetry structure models, such as $P6_3$ and $P\text{-}3$ [12, 15, 35]. It has been previously demonstrated that the lower symmetry is present in more complex systems, for which the A- and/or B- cation sites are occupied by more than one type of cation[14, 25]. In this case, the structure is more distorted as compared with $P6_3/m$. In the La-Si-O system, some low-symmetry structure models, such as $P6_3$ or even $P\text{-}3$, have been proposed[15], but these results have been open to question[12, 35], because all three structure models generate very similar powder diffraction patterns, and it is difficult to distinguish the subtle differences between these different models by powder XRD or neutron diffraction. In fact, the $P\text{-}3$ structure model may not be reliable because it has a slightly different extinction rule, and the (001) diffraction maximum was never observed in the synchrotron XRD patterns of this study. Single crystal XRD[13] results indicate that $La_{9.33}Si_6O_{26}$ apatite has a high symmetry $P6_3/m$ structure at ambient conditions. This was confirmed in this study by the combined use of synchrotron XRD and spectroscopic measurements. The pressure-induced reduction in symmetry of apatite structure is in agreement with a chemically-induced distortion in complex apatite systems[14]. Both XRD and spectroscopy measurements indicate that the low-symmetry apatite structure is not stable at ambient pressure and converts back to the high-symmetry phase upon pressure release.

The refinement of XRD patterns has indicated that there is a considerable proportion of cation vacancies in the sample, and the cation defects definitely generate anion defects, such as extra interstitial sites in the oxygen channels in apatite. XRD measurements do not allow one to

complete a quantitative analysis of these anion defects, especially in the high-pressure case, because of the weak x-ray scattering of oxygen. The defects in both the cation and anion sublattice of apatite may have a minor influence the observed phase transition. However, we suggest that the pressure-induced structural change is intrinsic to apatite structure, because we have observed similar phase transitions in single crystals of silicates and phosphates with the stoichiometric apatite structure.

Conclusions

We have observed, for the first time, a pressure-induced phase transition in $La_{9.33}Si_6O_{26}$ with the apatite structure ($P6_3/m$). The high-pressure phase has a lower symmetry, $P6_3$, which was determined by XRD, Raman scattering and infrared absorption measurements. The pressure-induced phase transition is intrinsic to lanthanide silicates with the apatite structure. The high-pressure phase of $La_{9.33}Si_6O_{26}$ has an abnormally low bulk modulus as compared with the higher symmetry, low-pressure phase. The large compressibility of the high-pressure phase is caused by the additional degree of freedom of the oxygen atoms that allows for tilting of the SiO_4 tetrahedron under increased pressure.

Acknowledgement

This work was supported by Materials Science of Actinides, an Energy Frontier Research Center funded by the U.S. Department of Energy, Office of Science, Office of Basic Energy Sciences under Award Number DE-SC0001089. The use of x-ray beam line at X17C and infrared at U2A station of NSLS is supported by NSF COMPRES EAR01-35554 and by US-DOE contract DE-AC02-10886.

* Corresponding author: rodewing@umich.edu

References

[1]M.J. Kohn, T.E. Cerling, Rev. Mineral Geochem. **48,** (455) 2002.

[2]G.H. McClellan, J.R. Lehr, Am. Miner. **54,** (1374) 1969.

[3]R.C. Ewing, P. Natl. Acad. Sci. USA **96,** (3432) 1999

[4]R.C. Ewing and W.J. Weber, *The Chemistry of the Actinides and Transactinide Elements*, Eds. L.R. Morss, N.M. Edelstein and J. Fuger (Springer, New York) **6,** (3813). (2010)

[5]T. Wakabayashi, S. Kato, Y. Nakahara, M. Ogasawara, S. Nakata, Catal. Today **164,** (575) 2011.

[6]L. Leon-Reina, E.R. Losila, M. Martinez-Lara, S. Bruque, M.A.G. Aranda, J. Mater. Chem. **14,** (1142) 2004.

[7]S. Ferdov, R.A. Sa Ferreira, Z. Lin, Mater. Chem. **18,** (5958) 2006.

[8] S. Nakayama, M. Sakamoto, J. Eur. Ceram. Soc. **18,** 1413 (1998).

[9]A. Orera, E. Kendrick, D.C. Apperley, V.M. Orera, P.R. Slater, Dolton Trans. 5296 (2008).

[10]J.E.H. Sansom, J.R. Tolchard, D. Apperley, M.S. Islam, P.R. Slater, J. Mater. Chem. **16,** 1410 (2006).

[11]A. Najib, J.E.H. Sansom, J.R. Tolchard, P.R. Slater, M.S. Islam, Dolton Trans. 3106 (2004).

[12]Y. Masubuchi, M. Higuchi, T. Takeda, S. Kikkwawa, Solid State Ionics, **177,** 263 (2006).

[13]H. Okudera, Y. Masubuchi, S. Kikkawa, A. Yoshiasa, Solid State Ionics, **176,** 1473 (2005).

[14]T.White, C. Ferraris, J. Kim, S. Madhavi, Rev. Mineral. Geochem. **57,** 307 (2005).

[15]J.E.H. Sansom, D. Richings, P.R. Slater, Solid State Ionics, **139,** 205 (2001).

[16]M.E. Fleet, Biomater. **30,** 1473 (2009).

[17]M. Snirnov, S. Sukhomlinov, A. Mirgorodsky, O. Masson, E. Bechade, M. Colas, T. Merle-Mejeau, I. Julien, P. Thomas, J. Raman Spectrosc. **41,** 1700 (2004).

[18]E. Rodriguez-Reyna, A.F. Fuentes, M. Maczka, J. Hanuza, K. Boulahya, U. Amaor, J. Solid State Chem. **179,** 522 (2006).

[19]J.R. Tolchard, M.S. Islam, P.R, Slater, J. Mater.Chem. **13,** 1956 (2003).

[20]L.W. Schroeder, M. Mathew, J. Solid State Chem. **26,** 383 (1978).

[21]K.N. Matsukage, S. Ono, T. Kawamoto, T. Kikegawa, Phys. Chem.. Miner. **31,** 580 (2004).

[22]P. Comodi, Y. Liu, P.F. Zanazzi, M. Montagnoli, Phys. Chem. Miner. **28,** 219 (2001).

[23]A. Hammersley, Computer program Fit 2d, ESRF, Grenoble (1998).

[24]T.Roisnel and J. Rodriguez-Carvajal,
Mat. Sci. Forum, Proc.7th Eur. Powder Diffr. Conf. (EPDIC7), 118 (2000).

[25]H.K. Mao, J. Xu, P.M. Bell, J. Geophys. Res. **91,** 4673 (1986).

[26]N. Kalsbeek, S. Larsen, Z. Kristallog. **191,** 249 (1990).

[27]L. Gerward, J.S. Olsen, J. Appl. Cryst. **30,** 259 (1997).

[28]J.E. Lowther, J.K. Dewhurst, J.M. Leger, J. Haines, Phys. Rev. B **60,** 14485 (1999).

[29]O. Ohtaka, D. Andrault, P. Bouvier, E. Schultz, M. Mezouar, J. Appl. Cryst. **38,** 727 (2005).

[30]J. Haines, J.N. Leger, A. Atouf, J. Am. Ceram. Soc. **78,** 445 (1995).

[31]S. Desgreniers, K. Lagarec, Phys. Rev. B**59,** 8467 (1999).

[32]R.M. Hazen, L.W. Finger, Am. Mineral. **64,** 196 (**1979)**.

[33]H.P. Scott, Q. Williams, E. Knittle, Phys. Rev. Lett. **88,** 015506 (2001).

[34]F.X. Zhang, V. Pointeau, L.C. Shuller, D.M. Reaman, M. Lang, Z. Liu, J. Hu, W.R. Panero, U. Becker, C. Poinssot, and R.C. Ewing, Am. Mineral. **94,** 916 (2009).

[35]L. Leon-Reina, E.R. Losilla, M. Martinez-Lara, S. Bruque, M.A.G. Aranda,
J. Mater. Chem. **14,** 1142 (2004).

[36]T.A. Mary, J.S.O. Evans, T. Vogt, A.W. Sleight, Science **272,** 90 (1996).

[37]F.X. Zhang, M. Lang, Z.X. Liu, R.C. Ewing, Phys. Rev. Lett. **105,** 015503 (2010).

Table I Structure of $La_{9.33}Si_6O_{26}$ apatite structure-type at 1bar and 15.2 GPa

P=1bar, space group: *P6₃/m* (#176)						P=15.2 GPa, space group: *P6₃* (#173)					
a=*b*=9. 6489(5)Å, *c*=7.1464(6)Å						*a*=*b*=9.286(3)Å, *c*=6.798(2)Å					
atom	site	x/a	y/b	z/c	SOF	atom	site	x/a	y/b	z/c	SOF
La1	*4f*	1/3	2/3	0.015(2)	0.76(2)	La1	*2b*	2/3	1/3	0.043(9)	0.70(7)
La2	*6h*	0.2296(7)	-0.0136(9)	1/4	0.99(1)	La2	*2b*	1/3	2/3	0.044(8)	0.75(7)
Si	*6h*	0.397(3)	0.369(4)	1/4	1.0	La3	*6c*	0.213(1)	-0.013(2)	0.267(7)	1.0
O1	*6h*	0.332(7)	0.489(7)	1/4	1.0	Si	*6c*	0.434	0.391	0.249	1.0
O2	*6h*	0.585(7)	0.485(7)	1/4	1.0	O1	*6c*	0.327	0.497	0.257	1.0
O3	*12i*	0.339(4)	0.256(4)	0.079(5)	1.0	O2	*6c*	0.604	0.464	0.279	1.0
O4	*2a*	0.0	0.0	1/4	0.95(1)	O3	*6c*	0.331	0.292	0.390	1.0
						O4	*6c*	0.358	0.264	0.027	1.0
						O5	*2a*	0.0	0.0	0.197	1.0

Table II The bulk modulus of the low-pressure and high-pressure polymorphs of some oxides

		TiO_2	ZrO_2	HfO_2	$ZrSiO_4$	$USiO_4$
	low P form	rutile: 230(20)[27]	baddeleyite: 157[28]	baddeleyite: 251[28]	zircon: 227[32]	coffinite: 188(4)[34]
B_0(GPa)	high P forms	α-PbO_2: 260(30)[27]	cotunnite: 278[29],332(8)[30] 444(15)[31]	cotunnite: 340(10)[31]	scheelite: 301.4(12.5)[33]	scheelite: 274(16)[34]

Figure Captions

Fig.1 Selected XRD patterns of $La_{9.33}Si_6O_{26}$ apatite structure-type at various pressures. A pressure-induced phase transition occurs at 13.3 GPa (see enlarged patterns on the right). The structure changed from $P6_3/m$ to $P6_3$. The spheres are La, and the polyhedra are SiO_4 tetrahedra

Fig.2 a) Rietveld refinement of the XRD patterns of $La_{9.33}Si_6O_{26}$ at 1bar with space group of $P6_3/m$ and at 15.2 GPa with space group of $P6_3$; The pressure dependence of a) unit cell volume; c-e) lattice parameters for $La_{9.33}Si_6O_{26}$ apatite structure-type. The *c*-axis and *c*/*a* values show an obvious discontinuity at the phase transition.

Fig.3 a) Raman spectra of $La_{9.33}Si_6O_{26}$ apatite structure-type at high pressures; b) Pressure dependence of the wavenumbers of Raman active modes. New modes (marked with arrows) for the high-pressure phase are due to the symmetry degradation.

Fig.4 a) Far-Infrared spectrum and b) Middle-IR spectrum of $La_{9.33}Si_6O_{26}$ apatite structure-type at high pressures.

Figure 1

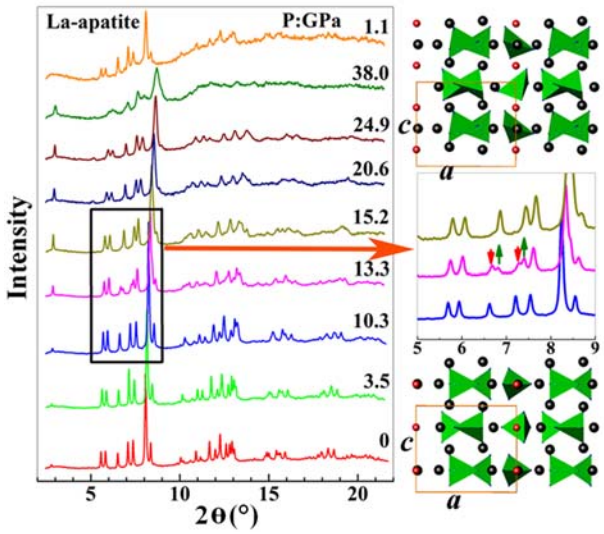
La-apatite
P:GPa
1.1
38.0
24.9
20.6
15.2
13.3
10.3
3.5
0
Intensity
5
10
15
20
2θ(°)
c
a
5
6
7
8
9
c
a

Figure 2

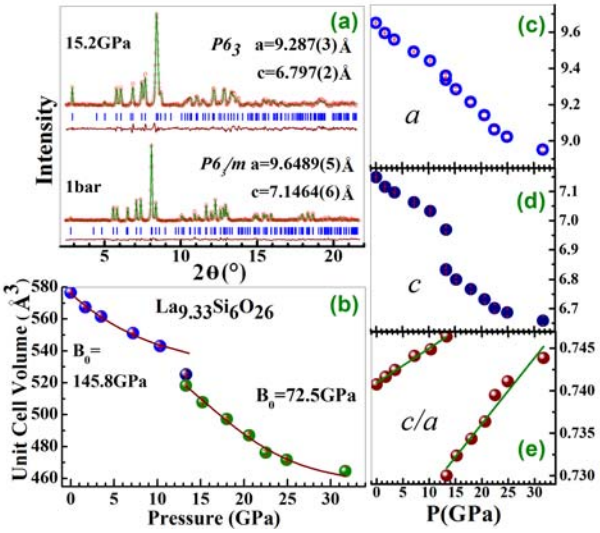
(a)
15.2GPa
P6₃ a=9.287(3)Å
c=6.797(2)Å
1bar
P6₃/m a=9.6489(5)Å
c=7.1464(6)Å
Intensity
2θ(°)
(b)
La9.33Si6O26
B0= 145.8GPa
B0=72.5GPa
Unit Cell Volume (Å3)
Pressure (GPa)
(c)
a
(d)
c
(e)
c/a
P(GPa)

Fig.3

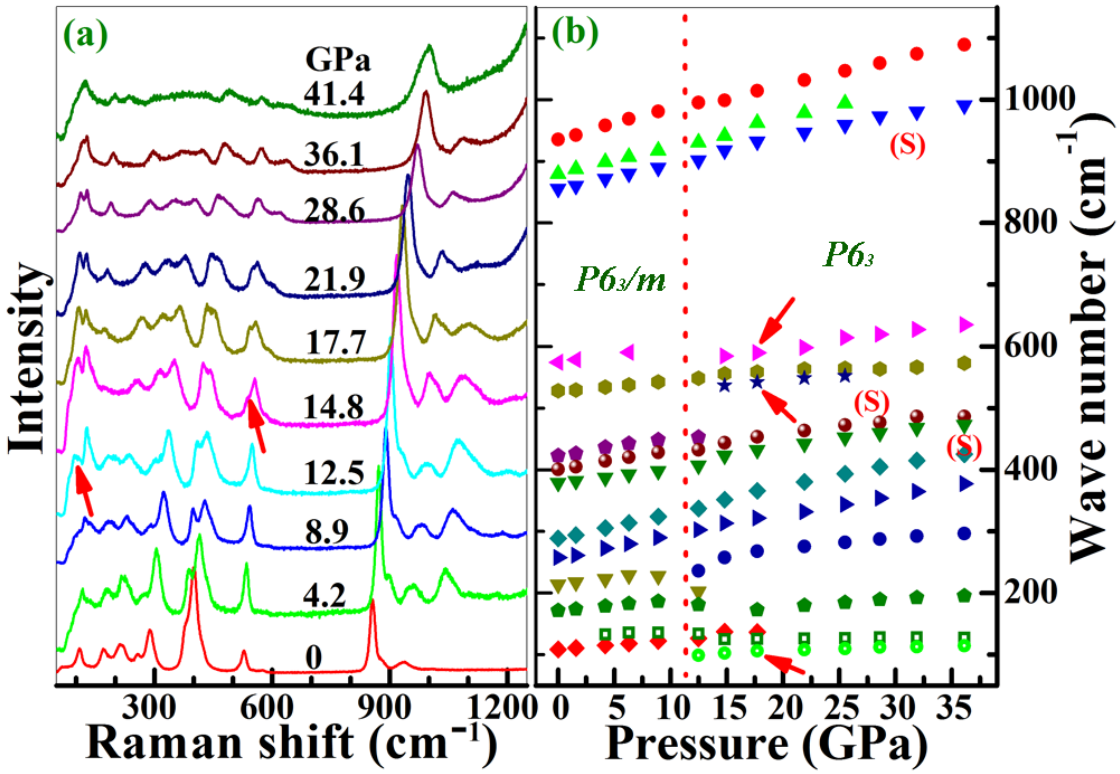
(a)
GPa
41.4
36.1
28.6
21.9
17.7
14.8
12.5
8.9
4.2
0
Intensity
300
600
900
1200
Raman shift (cm^{-1})
(b)
P6$_3$/m
P6$_3$
(S)
(S)
(S)
0
5
10
15
20
25
30
35
Pressure (GPa)
1000
800
600
400
200
Wave number (cm^{-1})

Fig.4

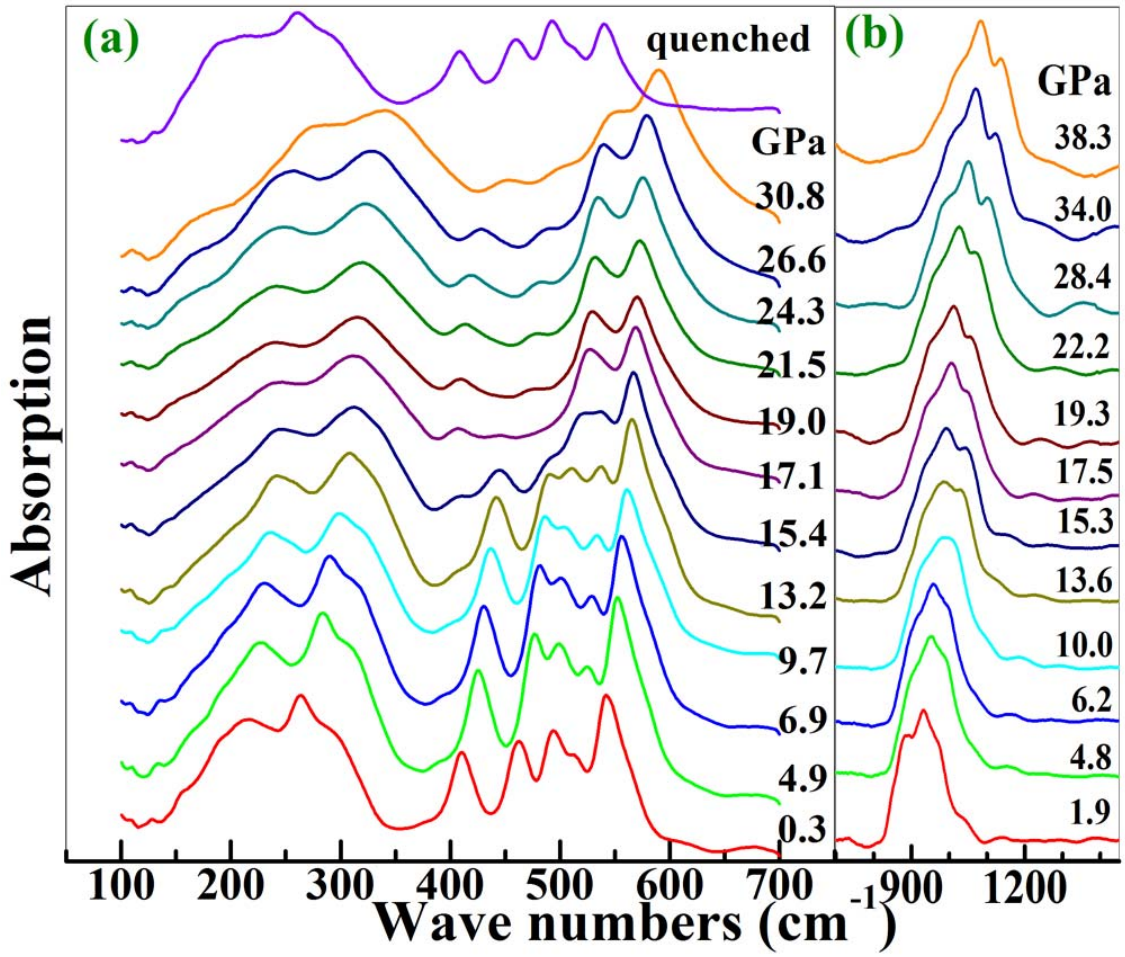
(a)
quenched
GPa
30.8
26.6
24.3
21.5
19.0
17.1
15.4
13.2
9.7
6.9
4.9
0.3
(b)
GPa
38.3
34.0
28.4
22.2
19.3
17.5
15.3
13.6
10.0
6.2
4.8
1.9
Absorption
100
200
300
400
500
600
700
900
1200
Wave numbers (cm-1)